Article

Journal of Vibration and Control
2018, Vol. 24(19) 4395–4406

DOI: 10.1177/1077546317724949
journals.sagepub.com/home/jvc
SAGE

Experimental validation of fail-safe hybrid mass damper

Simon Chesné[1] and Christophe Collette[2]

Abstract

A simple control law, dedicated to improving the performance and stability of hybrid mass dampers, is investigated. The resulting hybrid device is based on decentralized velocity feedback techniques. Two poles and two zeros are added to the initial control law, in order to interact with the dynamics of the structure and the actuator. The interest of these interactions is to change the poles of the closed loop system so as to make the controlled system *hyperstable*. The margins of gain and phase are therefore infinite. Consequently, the proposed hybrid system controller is fail-safe but also unconditionally stable in theory. Experimentation, using a tuned voice coil actuator, illustrates the performance and robustness of this hybrid control device.

Keywords

Tuned mass damper, active vibration control, hybridization, hyperstability, velocity feedback

1. Introduction

When a classical inertial actuator is used to actively control a structure, its resonance frequency is much lower than the fundamental resonance frequency of the controlled structure. Such a device is often called an Active Mass Damper (AMD). For applications such as in buildings, actuators have a very low stiffness. However, this may result in problems in the context of embedded applications such as in transportation vehicles (e.g., cars, helicopters or aircraft), which are subject to significant acceleration and deceleration transients. In this context, to avoid large deflections of the actuator's mass, the suspension stiffness has to be sufficiently high, thus increasing the fundamental resonance of the actuator. In order to add viscous damping to the structure, the natural way is to drive these actuators with a signal which is proportional to the velocity. However, for large values of the control gain, stability is no longer guaranteed, even when the structure velocity is measured near the AMD. It is believed that this is the reason why many elaborate control strategies have been introduced to control AMDs (although this is rarely openly confessed): classical tuning (Burgos et al., 2004), fuzzy controllers (Battaini et al., 1997; Movassaghi, 2012; Li, 2014), pole placement (Tso et al., 2013), Lyapunov's method (Kim et al., 2004), optimal control (Nishitani et al., 1996; Wang, 2009; Yoshida and Matsumoto, 2009; Qi et al., 2010), μ-synthesis (Liu et al., 1998), H-infinity (Baoya and Chunxiang, 2012), or sliding mode control (Thenozhi and Yu, 2014). Other approaches consider the problem of the proximity of the resonant frequency of the actuator to that of the controlled structure. To increase the stability margins of the control system, they introduce a compensator into the feedback loop Elliot and Rohlfing (2012) by actively softening the actuator. The resulting compensator poses no more restrictions on the fundamental resonant frequency of the actuator. But these compensators are usually based on the pole-zero cancellation principle and present some known dangers. Indeed when the pole-zero cancellation is not perfect, it can rapidly destabilize the control system.

Recently, a novel class of dampers has appeared that are trying to combine several objectives at the same time. These devices are gathered under the common

[1]CNRS INSA-Lyon, Université de Lyon, France
[2]BEAMS department, Université Libre de Bruxelles, Belgium

Received: 30 December 2016; accepted: 8 July 2017

Corresponding author:
Simon Chesné, Université de Lyon, CNRS INSA-Lyon, LaMCoS UMR5259, F-69621, France.
Email: simon.chesne@insa-lyon.fr

name of Hybrid Mass Dampers (HMDs), or Hybrid Vibration Absorbers (HVAs). In this paper, we focus on HMDs, which combine passive and active vibration control. The objectives are threefold: (1) increase performance, (2) reduce consumption, and (3) ensure a fail-safe behavior, that is, that the damper will work as a tuned mass damper when the controller is turned off. For example, in Yoshida and Matsumoto (2009), an HMD is presented where an optimal control is used to combine structural damping with a restricted stroke of the actuator. In Cheung et al. (2012), an H-infinity optimal control is used to minimize both the response and the control effort. In Rodriguez et al. (2016), an FXLMS controller is used to enhance the frequency range of an resonant isolation system for helicopter applications (SARIB[copyright]). In Tso et al. (2013), the control relies on the pole placement technique. In Preumont and Seto (2008), a dual loop approach is preferred to increase the stability margins. In Abe (2004), a two degree of freedom system is studied, which can behave as an AMD to suppress the vibrations induced by small earthquakes, and as a tuned mass damper to suppress the vibrations of a targeted mode excited by a big earthquake. In the active configuration, a linear quadratic regulator is used with a large gain on the structural velocity. The control is switched off above a threshold value of the structure displacement, that is, when the actuator cannot deliver the requested force anymore. One common feature of the aforementioned controllers is that they are model-dependent and that the control law is usually complex to tune. Thus their performance against parameter variations in the system is not very robust.

In order to bypass this limitation, this paper experiments a novel and simple control law previously introduced in Collette and Chesne (2016). It drastically improves the performance of classical hybrid dampers based on decentralized velocity feedback techniques. In this approach, a compensator is introduced in the control loop to correct the phase of the actuator in order that it becomes stable at low frequency. The interactions between the structure and the controller change the poles of the closed loop system so as to make the controlled system *hyperstable* (Collette and Chesne, 2016). The margins of gain and phase are therefore infinite. Consequently, the proposed hybrid system controller is fail-safe but also unconditionally stable in theory.

The paper is organized as follows. Section two briefly presents the concept of the control law named the α-controller and proposes an analysis of its performance and stability properties. Section three presents the setup used in the experimentation and particularly the HMD device. Section four presents and discusses the performance, limitations, and robustness of the new controller. Section five draws conslusions.

2. The α-hybrid mass damper

Consider a one degree of freedom system with a resonant frequency of $\omega_0 = \sqrt{k_1/m_1} = 1\,\text{rad.s}^{-1}$ without damping. The mechanical parameters are $m_1 = 1\text{kg}$, $m_2 = \mu m_1$ with $\mu = 0.01$ and $k_2 = m_2\omega_0\nu N.\text{m}^{-1}$ with $\nu = 1/(1+\mu)$ (see DenHartog, 1956). We associate to this system a classical dynamic vibration absorber (TMD without damping) with a mass ratio $\mu = 1\%$. Usually structures are lightly damped and the TMD has an optimal damping ratio. The choice is made here to consider a system without damping, it allows clearer illustration of the stability limits and the analysis of the phase. The model is illustrated in Figure 1. The resulting resonant frequencies of the system are named ω_1 and ω_2. Classical Direct Velocity Feedback (DVF) control generates a command to the actuator, proportional to the measured velocity of the main structure (represented by m_1). The application of a unitary force on a TMD used as an actuator results in the open loop transfer function and the root locus plotted in Figure 2 (dashed black lines). Analysis of the stability margins shows clearly the limitations of this approach. Below the first resonance frequency, as the phase is up to 180°, the system is stable only at very low feedback gain. One sees also on the root locus that the lower frequency pole goes immediately into the right half plane, leading to instability. The closed loop system will always be marginally stable. This is mainly due to the absence of a zero between the pole of the TMD and the pole of the structure. As explained in the introduction, several elaborations of the controller have been proposed to bypass this limitation. We propose here a simple alternative which addresses the stability and weak margins problem adequately by placing a pair of zeros at the right location, which will

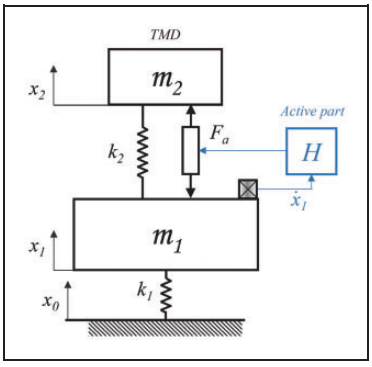

Figure 1. Scheme of the hybrid device without damping.

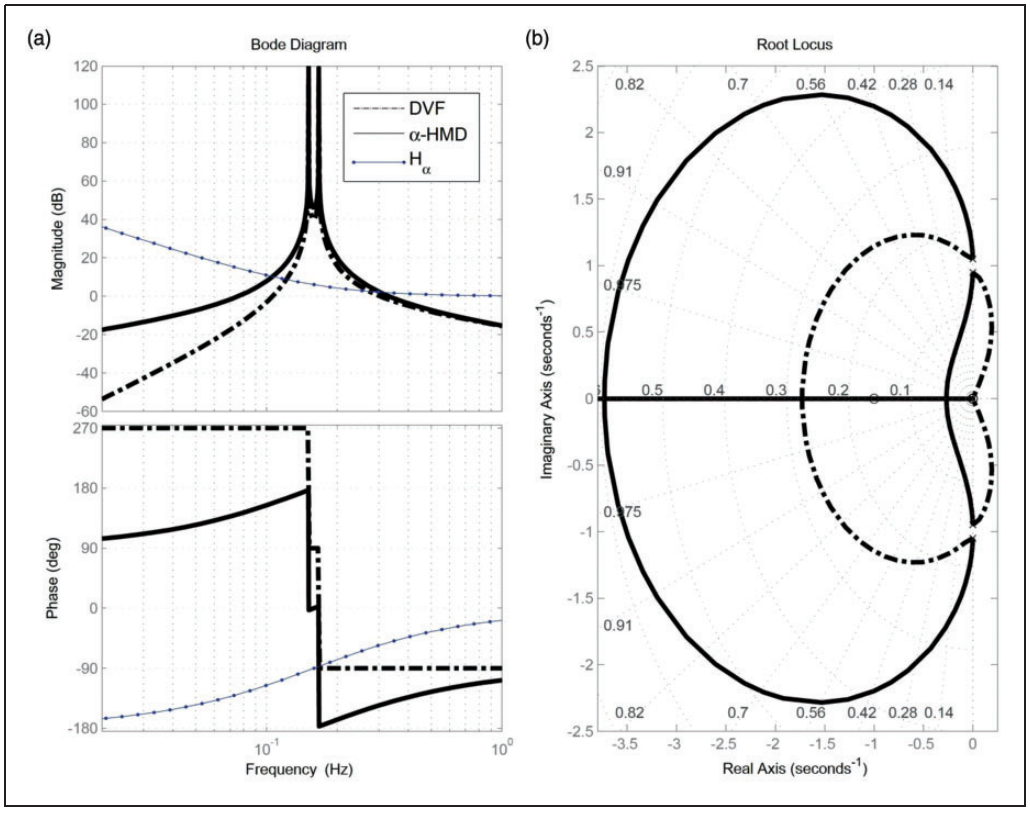

Figure 2. (a) Bode and (b) root locus plots of sensor-actuator open loop transfer function for Direct Velocity Feedback (black dashed line) and for α-controller using $\alpha = \omega_0$ (continuous black line). Transfer function $H_\alpha(s)$ in blue dotted line.

allow recovery of a guaranteed stability of the closed loop system.

We still consider a TMD tuned on the first mode as the actuator. The controller still uses velocity feedback; however, an α-controller filter is added into the control loop (Collette and Chesne, 2016)

$$H_\alpha(s) = g\frac{(s+\alpha)^2}{s^2} \tag{1}$$

One sees that a pair of poles and zeros have been introduced; consequently the phase has been modified below the first resonant frequency (see its transfer function in Figure 2(a), blue dotted line). The parameter α is tuned to make the controller hyperstable. Its value is $\alpha = \omega_0$ and corresponds to the resonant frequency of the initial structure without TMD. The tuning of gain g depends on the objectives of the controller and also on the capability of the transducer. In this example it is chosen as $g = 1$. The resulting root locus of the α-HMD is plotted in Figure 2(b) (black continuous line). Initially, the whole root locus plot is in the left half plane, meaning an unconditional stability of the feedback system (infinite gain margin). The open loop phase is always between -180° and 180°.

In Collette and Chesne (2016) it has been shown that the hyperstability limits for undamped system are

$$\omega_1 < \alpha < \omega_2 \tag{2}$$

Figure 3 shows the phase of the open loop transfer function for two extreme cases, along with the departures of the poles in the complex plane. One can understand it as a constraint on the departure angle of the root loci to keep the pole in the left half plane, or one can observe the phase of the open loop transfer function. For the two extreme cases ($\alpha = \omega_1$ and $\alpha = \omega_2$), the phases are tangential to the hyperstability limits (-180° and 180°) but stay inside the interval.

These representations are plotted considering a system without damping, to highlight the theoretical limits. Initial damping in the structure and in the TMD increase the stability margins considerably.

3. Experimental setup

3.1. Structure and transducer

The control device is represented in Figure 4. The TMD is by Micromega products, originally designed for

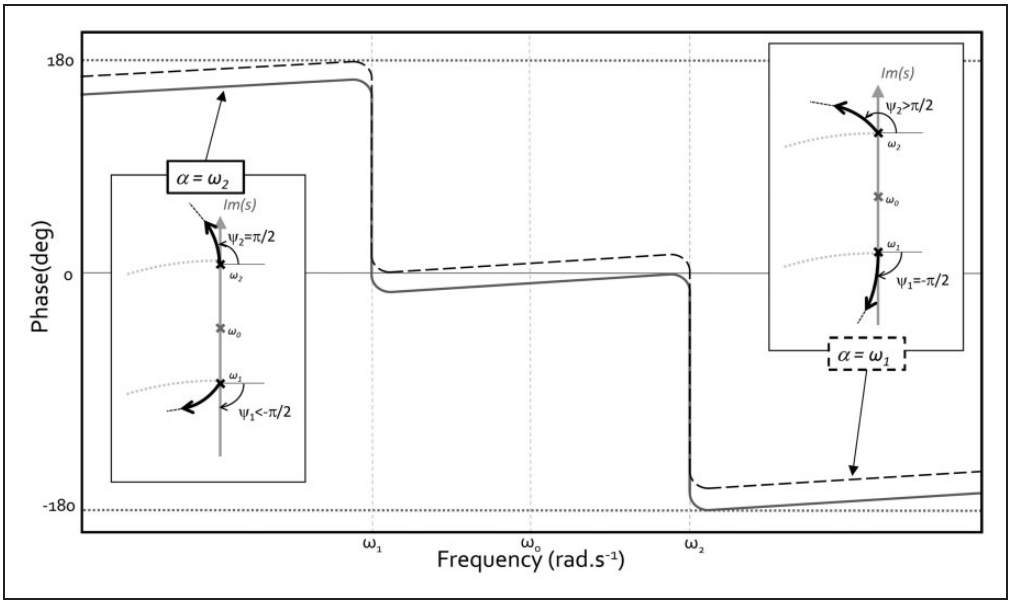

Figure 3. Phase representations of sensor-actuator open loop transfer function for α-controller using $\alpha = \omega_1$ and $\alpha = \omega_2$, and corresponding angle of departure on the root loci.

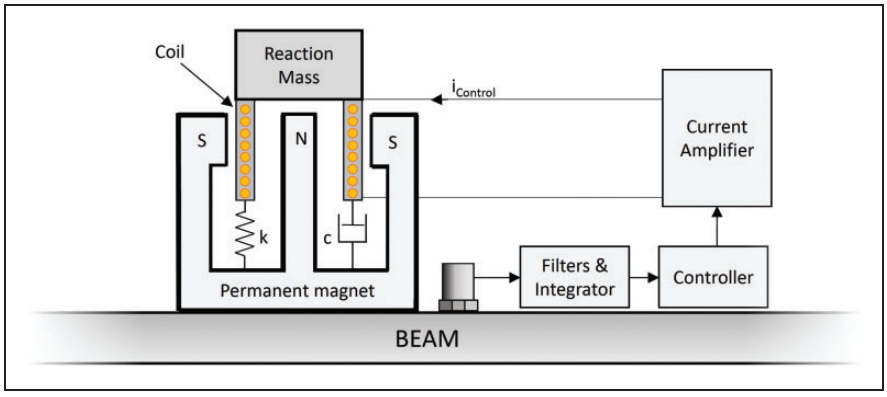

Figure 4. Schematic of the control device.

purely active control (ADD-5N; http://www.micro-mega-dynamics.com). Its moving mass is 160 g, its resonant frequency is around 21Hz, and its internal damping of $\xi = 11.9\%$. The experimental setup used for the validation is a cantilever steel beam (length: 58 cm, width: 10 cm, thickness: 1 cm). The damper is rigidly mounted on the beam, at a distance of $L_{hmd} = 48$ cm from the fixation. An accelerometer is fixed near to the actuator. The structure and the control device are shown in Figure 5. The targeted mode is the first bending mode of the beam. Thus, the dimensions of the beam have been chosen in order that the damper behaves as a TMD tuned on the first bending mode when the controller is turned off. In order to obtain a control force proportional to the command in the whole frequency band, the system is driven in current.

The mass ratio comparing the moving mass of the TMD and the effective modal mass of the flexible structure is $\mu = 9.4\%$. With this mass ratio, the theoretical optimal damping of the TMD should be $\xi_{opt} = 17.9\%$. The damping of the actual TMD is $\xi = 11.9\%$. In practice, neither the damping nor the resonant frequency are perfectly tuned to correspond to optimal values as defined in DenHartog (1956). Despite this, good performance is obtained showing the robustness of the approach as described in the following sections.

3.2. Practical considerations

To estimate the velocity in order to feed the controller, an acceleration sensor is used combined with an integrator. Consequently a high-pass (HP) filter is

introduced in the control loop to remove the DC terms. Moreover, the α controller law has two poles in zero (see Equation 1). This creates two new integration steps for the feedback signal. It may lead to an enhancement of the command at low frequencies, which may also lead to stroke/force saturation effects in the actuator. To counter this effect, another two HP filters are introduced. These HP filters are introduced just after the sensor, as shown in Figure 4. These modifications on the feedback loop produce a loss in the phase and gain margins. The theoretical hyperstability is then lost. Nevertheless, as shown in the next sections, phase and gain margins are always very high. They do not represent a limitation of the control system. The corner frequency of these filters and their orders depends clearly on the controlled system, transducer conception, and noise present in the control loop.

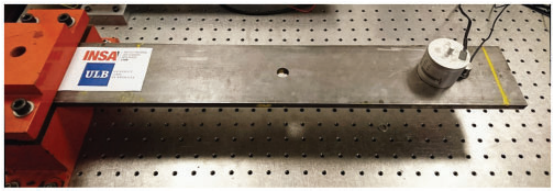

Figure 5. Picture of the experimental setup used to test the proposed controller. Cantilever beam, clamped at one end, and equipped with an AMD (Micromega Dynamics ADD-5N) at the other end. The motion of the beam is measured by a piezoelectric accelerometer, collocated with the AMD.

4. Experimental results

4.1. Open loop frequency response functions

Figure 6 shows the open loop transfer functions on the frequency band of interest in units of velocity over injected force. Without the α-controller, it corresponds to the open-loop transfer function of Direct Velocity Feedback (DVF). The DVF controller clearly shows its limitation as predicted by the theory with a gain margin of 7.5 dB at 18 Hz. But the main limitation appears on the closed loop response in Figure 7 (gray dotted line) where one can clearly see the dangerous increase of amplitude of the first peak as predicted by the root locus plot in Figure 3 or in Collette and Chesne (2016).

The α-controller has an antiresonance dip (double-zero) at the actuator's fundamental resonant frequency ($\alpha = \omega_0$), which compensates the phase below the actuator resonance with a 180° phase-advance. The resulting

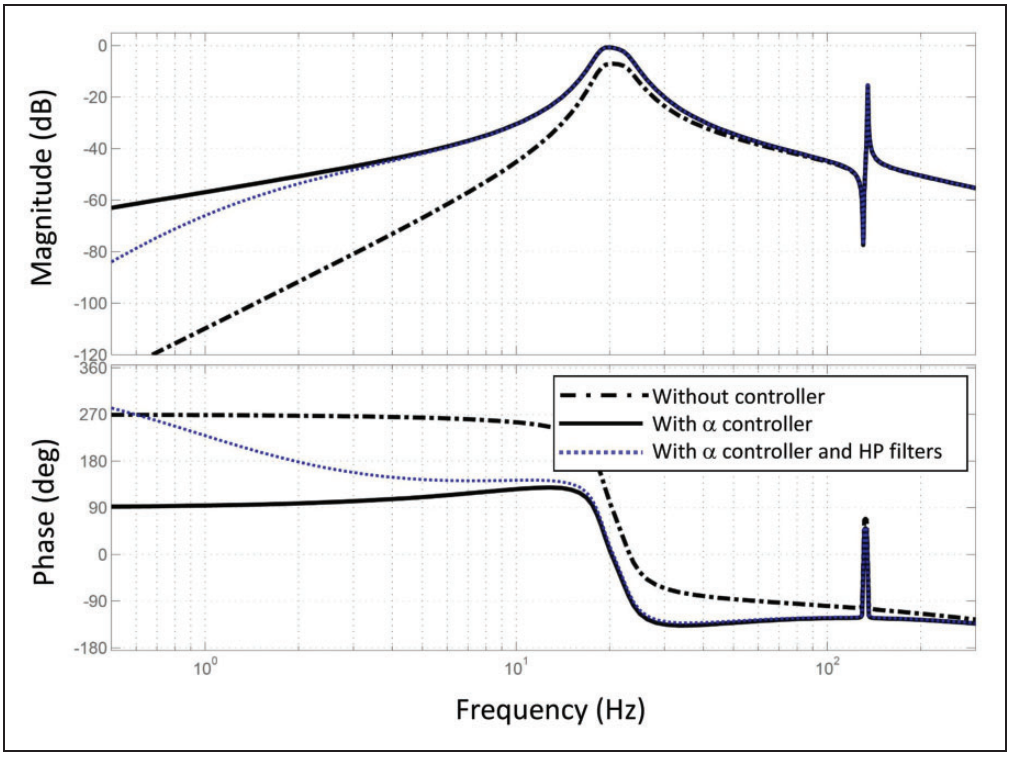

Figure 6. Bode plot of the sensor-actuator open loop transfer function without controller (black dashed line), with α-controller (black continuous line) and with the highpass filters (blue dotted line) ($f_c = 2 * \pi$ rad.s^{-1}).

open loop phase is then always between -180° and 180° equivalent to stability.

As explained earlier in the manuscript, the main drawback of the proposed controller is the enhancement at low frequencies creating limitations of the feedback gain and an important DC component. Three HP filters at 1Hz are added into the loop. The theoretical hyperstability is lost, but the resulting gain margin is 54dB at 2Hz. In practice, this kind of gain is so high that is not reachable.

4.2. Performance

The performance of the control device is observed in terms of the velocity response at the accelerometer location. Figure 7 shows the velocity response of the beam without TMD (gray continuous line), with passive TMD (black line), with DVF (gray dotted line), and with the α-controller using various gains ($g=1$ in blue, $g=3$ in purple, and $g=9$ in red). The effect of the DVF has already been commented on in the previous section. One can easily observe the effect of the α-controller on the first mode. Depending on the gain, it can reach a huge attenuation in comparison to the passive device.

Figure 8 shows the root locations for various values of the gain ($g=1$, 3, and 9) compared with the root locus predictions of the α-controller without (black continuous line) and with (blue dotted line) the HP filters. This figure shows a good correlation between model and experiment. Analyzing the root locus in detail, one can see that the system is very stable even with the HP filters. Indeed, the effect of the modifications linked to the use of these filters appears on the root locus only at very high gains and at low frequencies. It also shows that damping can be added on both poles. Consequently, the effect of these filters does not modify the behavior or limit the performance of the control device proposed in this study. The damping on the first mode without TMD is 0.24%; with passive TMD it reaches around 9% due to the important mass ratio, and with the α-controller it increases to more than 16% for both peaks.

The proposed control law presents the advantage of a wide frequency range effect, as has been demonstrated in Collette and Chesne (2016). The effect on the second mode is observable on a zoom of the response in Figure 9 with an attenuation of 7.3dB for $g=9$. This wide frequency range effect is also observable on the third mode and can be more easily seen on the cumulative RMS value of the velocity over $[0-500]$Hz. One sees that even for small gains, the response reduces quickly, and the effect on the integrated RMS value is important.

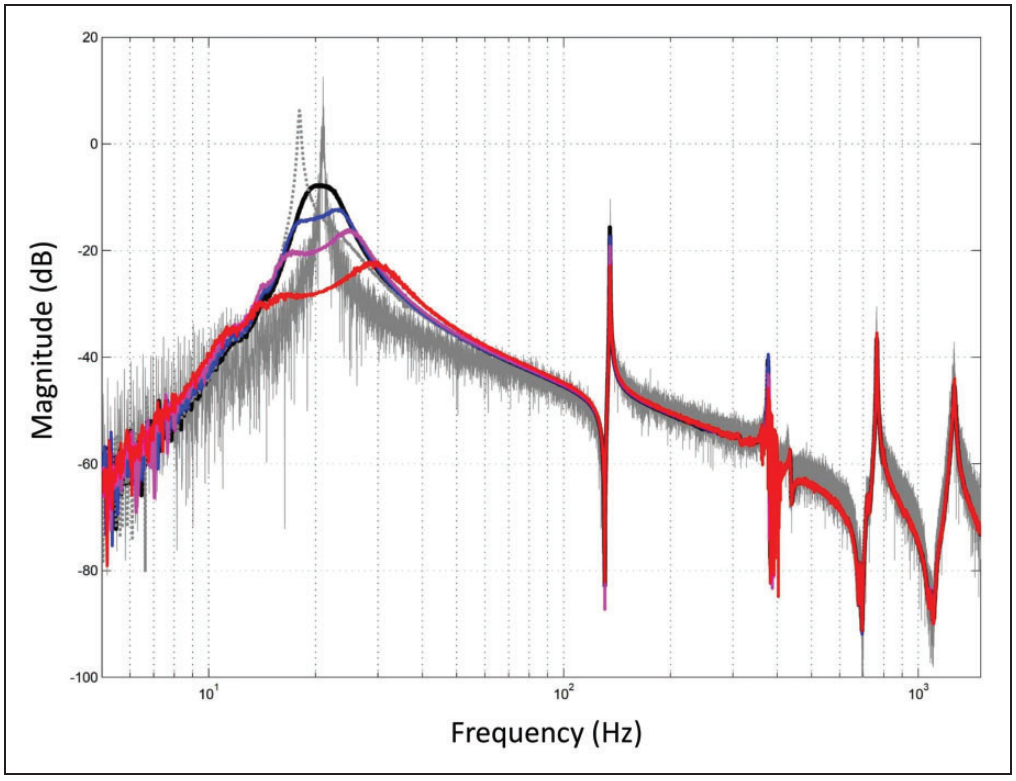

Figure 7. Frequency response functions, without control (gray), with passive TMD (black), with DVF (gray dotted line) and with α-controller using various gains ($g=1$ in blue, $g=3$ in purple, $g=9$ in red).

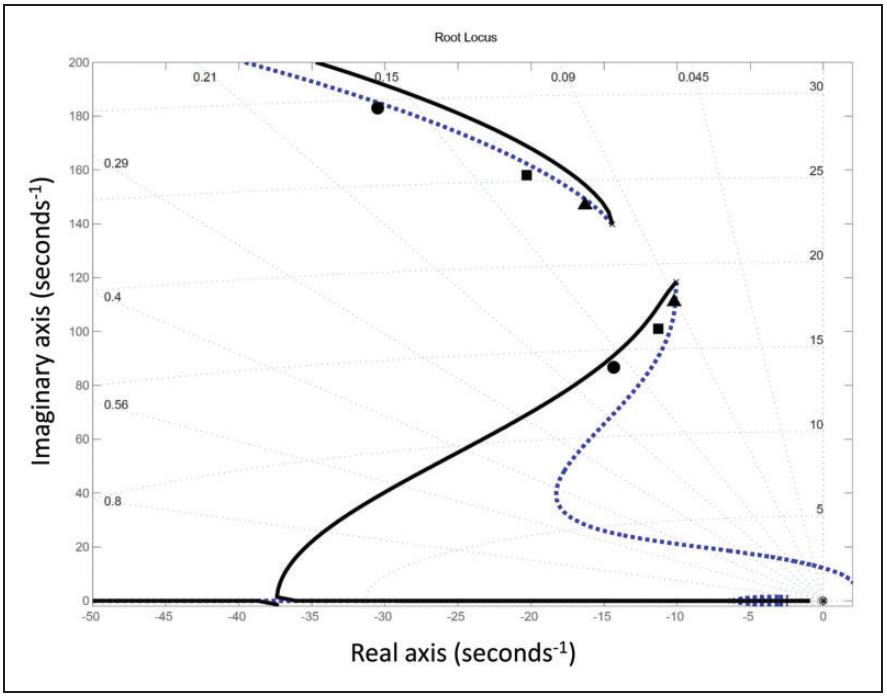

Figure 8. Root locus of the α-controller as a function of the control gain (black continuous line) with the highpass filters (blue dotted line), and experimental poles depending on the gain (▲ $g = 1$, ■ $g = 3$, • $g = 9$).

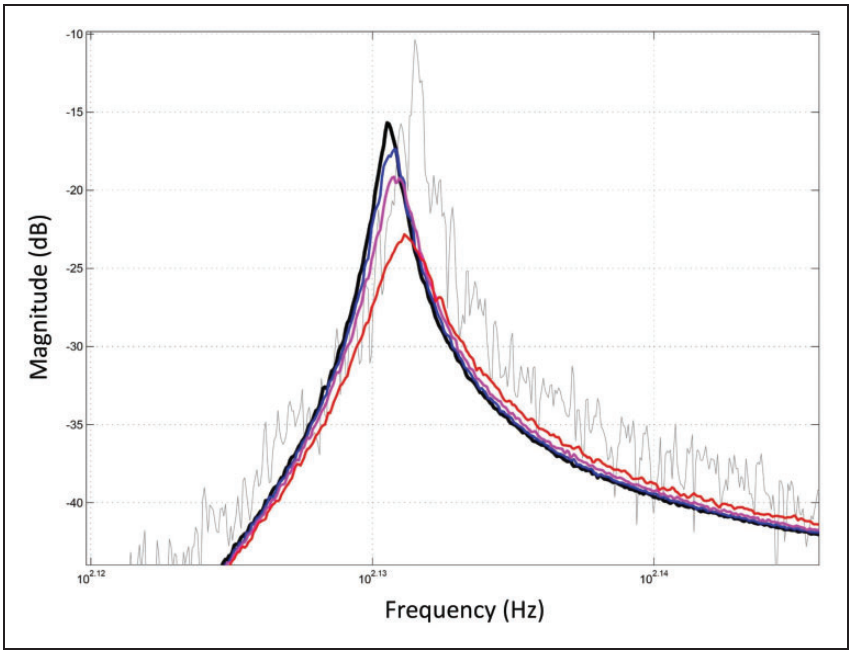

Figure 9. Zoom on the second mode of the frequency response functions, without control (gray), with passive TMD (black) and with α-controller using various gains ($g = 1$ in blue, $g = 3$ in purple, $g = 9$ in red).

Another point of view from which to analyze this hybrid device is to examine the actuator stroke. It is known that the stroke of a passive TMD is directly linked to the dissipated energy. Figure 11 shows a reconstruction of the stroke for the passive (black continuous line) and for the hybrid (blue dotted line) devices for a normalized impact at the free boundary of the beam. Note that the actuator stroke cannot

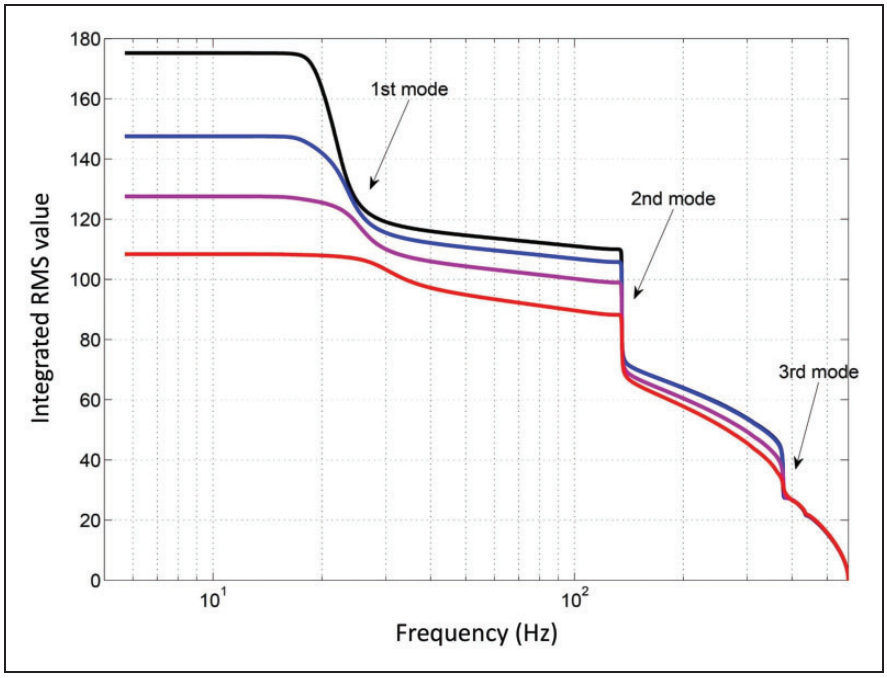

Figure 10. Integrated RMS value $[0 - 500]$Hz of the frequency response functions with passive TMD (black) and with α-controller using various gains ($g = 1$ in blue, $g = 3$ in purple, $g = 9$ in red).

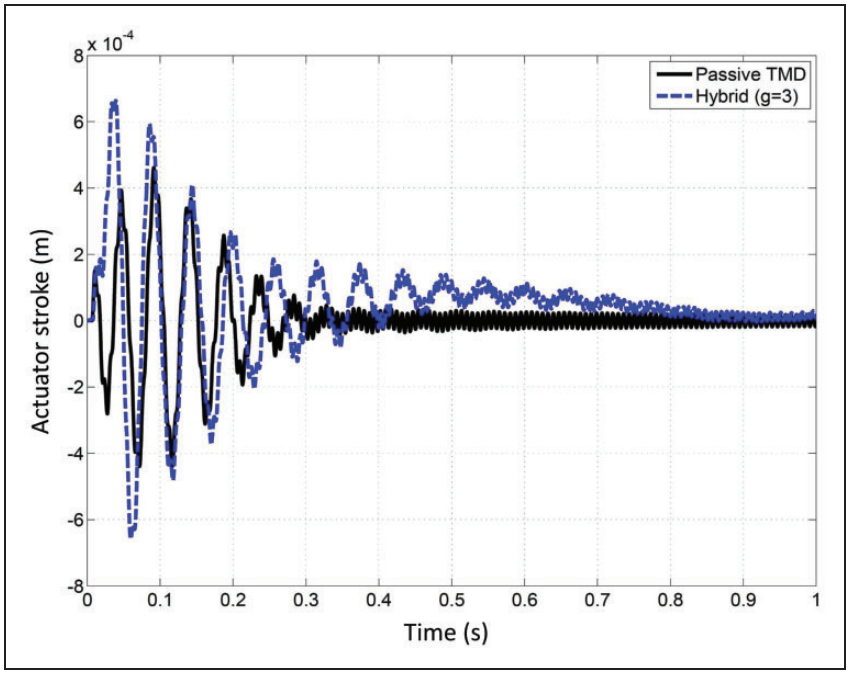

Figure 11. Actuator Stroke reconstruction, passive TMD (continuous black line) and hybrid one (blue dotted line, $g = 3$).

be directly measured on this device. Consequently, an experimental model feed with measured data (Impact force and resulting acceleration of the beam) is used to reconstruct the resulting actuator stroke. One can see that the hybrid device presents a larger stroke than the passive one, leading to the vibration reduction previously observed. The small offset observed at around 0.5s is due to the various integration steps of the signal. As the HP filters are tuned to $f_c = 1$Hz, more time is needed to stabilize the

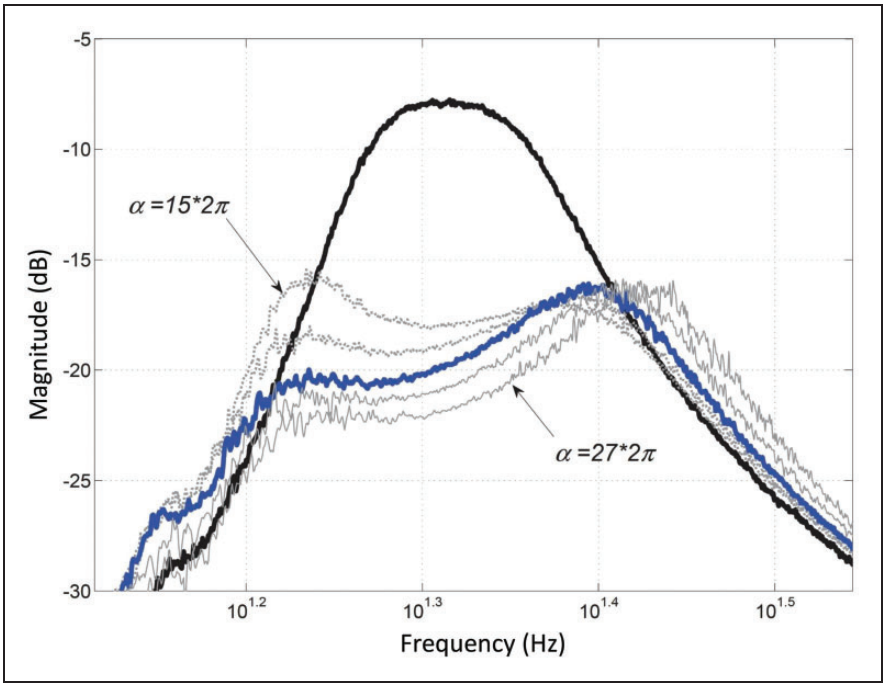

Figure 12. Velocity response on the first mode with passive TMD (black continuous line), with various α-controllers using $g = 3$. Gray dotted line: $\alpha = 15 * 2\pi$ and $18 * 2\pi$, blue continuous line: $\alpha = 21 * 2\pi$, gray thine line: $\alpha = 24 * 2\pi$ and $27 * 2\pi$.

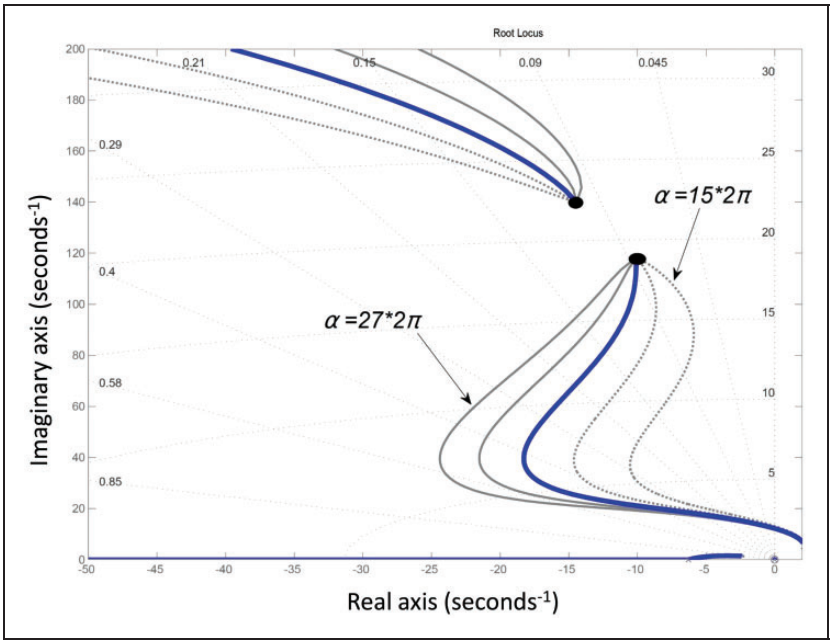

Figure 13. Root locus variations around the first mode with various α-controllers using $g = 3$. Gray dotted line: $\alpha = 15 * 2\pi$ and $18 * 2\pi$, blue continuous line: $\alpha = 21 * 2\pi$, gray thin line: $\alpha = 24 * 2\pi$ and $27 * 2\pi$.

command around zero. One of the most important advantages of the hybrid device can be observed in this figure, which is that the maximum stroke of the actuator is reached at the first oscillation of the moving mass. This means that the active part of the system helps the absorber to start its movement. This is in contrast to the passive device where it can take time to reach the maximum stroke to dissipate energy; in this case the actuator needs three oscillations to reach its maximum.

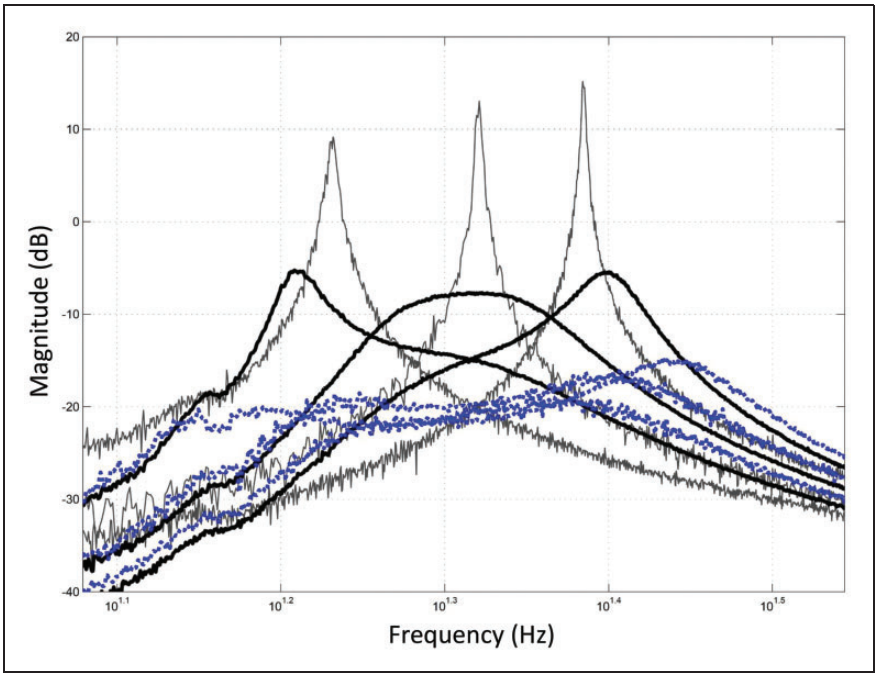

Figure 14. Velocity response on the first mode without TMD (gray thine lines), with passive TMD (black continuous lines), with α controller (blue dotted lines) using $\alpha = 21 * 2\pi$ and $g = 3$, for different length of the beam.

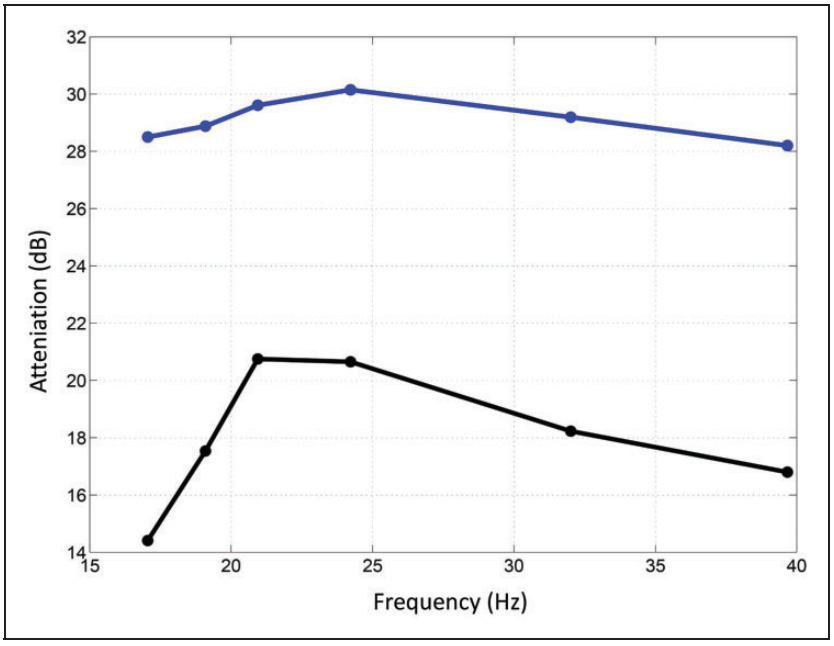

Figure 15. Attenuation obtained for various length of the cantilever beam using a passive TMD (black line) and a hybrid one (blue line).

To sum up, by looking at Figure 11, we can understand that the active part increases the stroke of the actuator and helps its start. This last advantage can be of great utility in the case of nonlinear systems or to stop structural instabilities.

4.3. Robustness analysis

The robustness of the α-controller is analyzed through the variation of two parameters: (i) a variation of the tuning parameter α in the control loop and (ii) a variation

of the resonance frequency of the structure. In a previous paper, Collette and Chesne (2016) advise tuning the α-parameter equal to the focused resonant frequency of the main structure. Consequently, for the experimental validation presented here, $\alpha = 21 * 2\pi$ has been chosen.

The effect on the amplitude attenuation of detuning α can be seen on the spectra plotted in Figure 12 ($\alpha = 15$, 18, 21, 24 and 27 with $g = 3$). Even if these variations represent and error greater than ±30% on the optimal theoretical value, the attenuation performance remains very good. The stability is also not fundamentally modified as illustrated in Figure 13. Indeed, for the worst case, ($\alpha = 27 * 2\pi$), the gain margin is 50dB at 2Hz. No effect can be observed on higher order modes.

In order to change the resonance of the main structure, the length of the cantilever beam has been modified. Six different lengths ($L = 41$cm, 46cm, 53 cm, 58 cm, 61 cm, and 65 cm) have been tested leading to six different resonant frequencies ($f_0 = 39.6$Hz, 32Hz, 24.2Hz, 21Hz, 19Hz, and 17Hz). The frequency responses are plotted in Figure 14 for only three different lengths (53cm, 58cm,and 61cm), for better readability. The figure compares the velocity response without TMD, with passive TMD and with the α-controller ($\alpha = 21$ and $g = 3$). The passive TMD is affected by the detuning, and one of its poles rises in consequence. The α-controller smooths these variations, and the amplitudes of the responses are still very low. The Figure 15 sums up these tests by plotting the resulting attenuation with TMD and the α-HMD. The reference value is the case without TMD. While the efficiency of the TMD fades out rapidly when it is detuned, the α-HMD maintains an outstanding efficiency (more than 28dB even with a 50% detuning of the primary structure).

5. Conclusions

This paper has presented an experimental validation of a robust hybrid mass damper that combines two features: unconditional stability and a fail-safe characteristic. Moreover, it has been shown that it responds rapidly, which is an asset for applications in the aerospace industry. The control law has been presented and validated experimentally. Its robustness has been tested and discussed.

Declaration of Conflicting Interests

The author(s) declare that there are no potential conflicts of interest with respect to the research, authorship, and/or publication of this article.

Funding

The author(s) disclosed receipt of the following financial support for the research, authorship, and/or publication of this article: This work was supported by the F.R.S.–FNRS.

References

Abe N (2004) Passive and active switching vibration control with pendulum type damper. In: *Proceedings of the IEEE international conference on control applications*, Taipei, Taiwan, 2–4 Sept. 2004, Vol. 2, pp. 1037–1042.

Battaini M, Casciati F and Faravelli L (1997) Implementing a fuzzy controller into an active mass damper device. In: *American control conference*, Albuquerque, USA, 6 June 1997, Vol. 2, pp. 888–892.

Baoya C and Chunxiang L (2012) Design of active tuned mass damper based on robust control. In: *Computer science and automation engineering (CSAE), 2012 IEEE international conference*, Zhangjiajie, China, 25–27 May 2012, Vol. 2, pp. 760–764.

Burgos O, Hizon J and Sison L (2004) Comparison of classical and fuzzy control in active mass damping of a flexible structure using acceleration feedback. In: *TENCON, 2004 IEEE region 10 conference*, Chiang Mai, Thailand, 24 Nov. 2004, Vol. 4, pp. 645–648.

Cheung Y, Wong W and Cheng L (2012) Design optimization of a damped hybrid vibration absorber. *Journal of Sound and Vibration* 331(4): 750–766.

Collette C and Chesne S (2016) Robust hybrid mass damper. *Journal of Sound and Vibration* 375: 19–27.

Elliott SJ and Rohlfing J (2012) Multifunctional design of inertially-actuated velocity feedback. *Journal of Aoustical Society of America* 131(2): 1150–1157.

DenHartog J (1956) *Mechanical Vibrations*, 4th ed. New York: Mc Graw-Hill.

Kim C, Hong K and Lodewijks G (2004) Anti-sway control of container cranes: an active mass-damper approach. In: *SICE 2004 annual conference*, Sapporo, Japan, 4–6 Aug. 2004, Vol. 1, pp. 939–944.

Liu D, Mao J and Zhang J (1998) Structure control with stiffness uncertainty in earthquake zone. In: *Control applications, 1998. Proceedings of the 1998 IEEE international conference*, Trieste, Italy, 4 Sept. 1998, Vol. 1, pp. 393–397.

Movassaghi Z (2012) Considering active tuned mass dampers in a five storey structure. In: *Control conference (AUCC), Sydney, Australia*, 15–16 Nov. 2012, pp. 320–323.

Nishitani A, Nitta Y and Yamada N (1996) Variable gain-based structural control considering the limit of amd movement. In: *Decision and control, 1996. Proceedings of the 35th IEEE conference*, Kobe, Japan, 13 Dec. 1996, Vol. 1, pp. 185–190.

Preumont A and Seto K (2008) *Active control of Structures*. West Sussex, United Kingdom: John Wiley and sons.

Qi S, Lu W, Chen P, Ming L, Ding D and He J (2010) Study on cable-stayed bridge flutter active control by a single group of adm. In: *Computing, control and industrial engineering (CCIE), 2010 international conference*, Wuhan, China, 5–6 June 2010, Vol. 2, pp. 426–430.

Rodriguez J, Cranga P, Chesne S and Gaudiller L (2016) Hybrid active suspension system of a helicopter main gearbox. Journal of Vibration and Control *July* 2016: 1–19.

Rohlfing J, Elliott SJ and Gardonio P (2012) Feedback compensator for control units with proof-mass electrodynamic actuators. *Journal of Sound and Vibration* 331: 3437–3450.

Thenozhi S and Yu W (2014) Fuzzy sliding surface control of wind-induced vibration. In: *Fuzzy systems (FUZZ-IEEE), 2014 IEEE international conference*, Beijing, China, 6–11 July 2014, pp. 895–900.

Tso M, Yuan J and Wong W (2013) Design and experimental study of a hybrid vibration absorber for global vibration control. *Engineering Structures* 56: 1058–1069.

Wang H-H (2009) Optimal vibration control for offshore structures subjected to wave loading with input delay. In: *Measuring technology and mechatronics automation, 2009. ICMTMA '09 international conference*, Hunan, China, 1–12 April 2009, Vol. 2, pp. 853–856.

Yoshida K and Matsumoto I (2009) Vibration suppression control for a multi-degree-of-freedom structural system using an amd with restricted stroke. In: *Networking, sensing and control. ICNSC '09 international conference*, Okayama, Japan, 26–29 March 2009, pp. 912–917.